FE NATURAL GAS CONTAINERS ANALYSIS AND EVALUATION

De Aguiar, José Manoel, josemaguiar@gmail.com
Tecnologia Mecânica, Faculdade de Tecnologia de São Paulo, FATEC-SP.
De Aguiar, João Batista, jbaguiar@usp.br
Sistemas Mecânicos, Escola Politécnica, Universidade de São Paulo

Abstract. *Natural gas containers design evolved from previous GLP applications. However, for transportation purposes, space and weight limitations required some shape optimization and the development of high strenght materials. A shell modelling for the stresses and deformations of metallic natural gas containers has been implemented as well as a solid modelling. A finite element simulation was developed and an alternative Fourier series solutions was considered. The stresses and deformations for the hemispherical shell , the nozzle intersection and the cylindrical shell are presented.*

Keywords *Shell, Elasticity, FEM, Fourier*

1. INTRODUCTION

Vehicular natural gas containers, in general, have numerous geometric discontinuities. The loading conditions normally are the internal pressure, some random external forces and thermal loads. The impact loads require a higher safety factor. The design of the containers is governed by official standards, codes and manufacturing requirements. The main concern is the high safety operation of the containers (Webster, Craig, 2001).

There are several international manufactures of cylindrical containers for natural gas. Historically (Mannesmann Cylinder Systems, 2007), the first containers were made of steel tubes. Later aluminum tubes were used in order to decrease cylinder weight. The cylinders made out of metal core are known as type I. At the beginning of 1990, composite cylinder products were developed. The steel composite cylinders, known as type II, have a seamless liner of chrome molybdenum steel for gas containment wrapped with carbon fiber. The metal lined fully wrapped, known as type III, has a metal for gas containment and is fully wrapped by a composite. The full composite cylinders, known as type IV, have a plastic liner, for gas containment, with a full glass fiber wrapping.

The fabrication process of type I containers normally uses chrome molybdenum seamless steel tubes. After the hemispherical ends are made, the chrome molybdenum steel suffers thermal treatment to improve mechanical characteristics. Latter, the nozzle end is machined and the containers cleaned. The hydraulic test is made with an internal pressure of 1.5 times the working pressure. Ultra sound inspection is done to verify superficial imperfections and possible leaks are verified by the nitrogen test.

A fem analysis was performed using 2D shell elements models and 3D solid element model. It is expected that the stress state in sectors with geometrical discontinuities, like nozzle intersections, curvature discontinuities, will have stress singularities (Sang, Z. F *et al*, 2002). Furthermore, certainly inaccuracies will be present, especially due to the difficulty of modeling complex geometric transitions,

2. Metal Cylindrical Gas Containers

The example chosen is a typical commercial cylindrical gas container as shown in Fig. 1. The main dimensions are the external diameter of 244 mm, length of the cylindrical sector of 850 mm. The thickness of most gas containers is in the range of 8 mm to 10 mm. (Cilibras, 2007). The cylinder is made of seamless chrome molybdenum steel tube. The re-laminated steel seamless steel tube fabrication process assures significant weight reduction. The model assumed the material properties corresponding to AISI 4130. The material properties and average composition are presented in Tab. 1 (Matweb, 2007). The aluminum gas containers weight one third of the corresponding steel containers (Dynetek, 2001). For the aluminum gas containers, the model assumes the Aluminum AA-6061-T6 and the properties are presented in Tab. 2 (Matweb, 2007). The low weight of aluminum gas containers makes them appropriate for scuba diving.

Material Composition AISI 4130 Wt. %								Tensile Properties			
C	Cr	Fe	Mn	Mo	P	S	Si	S_y	S_u	E	ν
0.28 0.33	0.80 1.10	97.3 98.2	0.40 0.60	0.15 0.25	Max 0.035	Max 0.04	0.15 0.35	460 MPa	560 MPa	205 GPa	0.29

Table 1. Chemical composition and mechanical properties AISI 4130

Material Composition AA 6061-T6 Wt. %								Tensile Properties			
Al	Cr	Fe	Cu	Mg	Mn	Si	Zn	S_y	S_u	E	ν
95.8 98.6	0.04 0.35	Max 0.7	0.15 0.40	0.80 1.20	Max 0.15	0.40 0.80	Max 0.25	276 MPa	310 MPa	68.9 GPa	0.33

Table 2. Chemical composition and mechanical properties AA-6061-T6

The nozzle has a valve for the input and output of the gas. The nozzle length used in the modeling had 80 mm long and external diameter of 50 mm. The hydraulic volume capacity of the cylinder is 30 liters. The container is certified under ISO 4705 D. The commercial denomination is Model 30244850 V ou 244.030.205D (Gifel, 2007). The service pressure is 200 bar. The cylinders are supported by cylindrical straps. The cylinders are normally placed in horizontal position inside or under the vehicle.

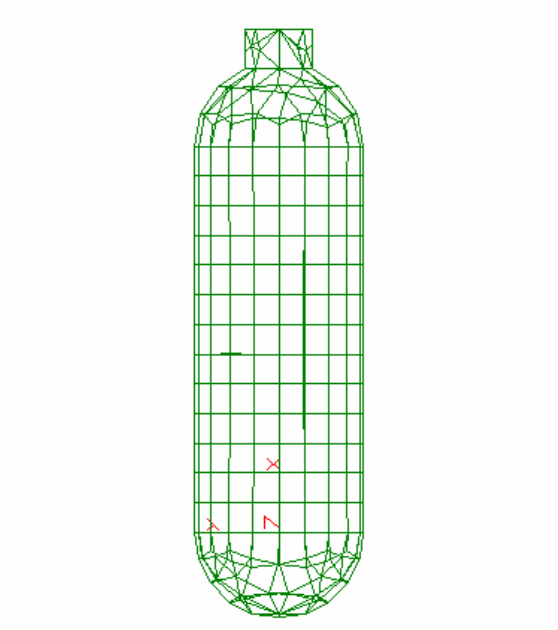

Figure 1. FE shell mesh model of Cylindrical Gas Container Model 30244850

2.1. Shell Equations

The gas container is formed by a spherical shell at the ends of the container and a cylindrical shell along the main body length and a cylindrical nozzle. For the case of small deformation, Flügge´s equations for the equilibrium of the shell middle surface are considered the most complete.

For the case of spherical shells, the equilibrium equations (Voyiadjis, George Z., Woelke, Pawel, 2004a) are:

$$\frac{\partial}{\partial\phi}(N_\phi \sin\phi) + \frac{\partial N_{\theta\phi}}{\partial\theta} - N_\theta \cos\phi - Q_\phi \sin\phi + R\sin\phi\, p_\phi = 0 \tag{1}$$

$$\frac{\partial}{\partial\phi}(N_{\theta\phi} \sin\phi) + \frac{\partial N_\theta}{\partial\theta} + N_{\theta\phi} \cos\phi - Q_\theta \sin\phi + R\sin\phi\, p_\theta = 0 \tag{2}$$

$$N_\theta \sin\phi + N_\phi \sin\phi + \frac{\partial Q_\theta}{\partial\theta} + \frac{\partial}{\partial\phi}(Q_\phi \sin\phi) - R\sin\phi\, p_z = 0 \tag{3}$$

$$\frac{\partial}{\partial\phi}(M_\phi \sin\phi) + \frac{\partial M_{\theta\phi}}{\partial\theta} - M_\theta \cos\phi - RQ_\phi \sin\phi = 0 \tag{4}$$

$$\frac{\partial}{\partial \phi}(M_{\theta\phi}\sin\phi)+\frac{\partial M_{\theta}}{\partial \theta}+M_{\theta\phi}\cos\phi-RQ_{\theta}\sin\phi=0 \tag{5}$$

$$\frac{M_{\phi\theta}}{R}-\frac{M_{\theta\phi}}{R}=N_{\phi\theta}-N_{\theta\phi} \tag{6}$$

In the equilibrium equations above, p_{ϕ}, p_{θ} and p_{z} are the equivalent distributed loads on the middle surface of the shell. The stress resultants $(N_{\theta},N_{\phi},N_{\theta\varphi},Q_{\theta},Q_{\phi})$ and associated couples $(M_{\theta},M_{\phi},M_{\theta\phi})$ may be expressed in terms of the displacements and rotations to produce the generalized displacement form of the equilibrium equations of spherical shells. The generalized stress resultants corresponding to thick shells can be introduced above to obtain the equilibrium equations for thick spherical shells.

For the case of cylindrical shells the equilibrium equations, in terms of the stress resultants and associated couples and external loading, are:

$$\frac{\partial N_{x}}{\partial \bar{x}}+\frac{1}{2}\left(\frac{\partial N_{x\theta}}{\partial \theta}+\frac{\partial N_{\theta x}}{\partial \theta}\right)+\frac{1}{2R}\frac{\partial M_{\theta x}}{\partial \theta}+R\,p_{x}=0 \tag{7}$$

$$\frac{1}{2}\left(\frac{\partial N_{x\theta}}{\partial \bar{x}}+\frac{\partial N_{\theta x}}{\partial \bar{x}}\right)+\frac{\partial N_{\theta}}{\partial \theta}+Q_{\theta}-\frac{1}{2R}\frac{\partial M_{\theta x}}{\partial \bar{x}}+R\,p_{\theta}=0 \tag{8}$$

$$\frac{\partial Q_{x}}{\partial \bar{x}}+\frac{\partial Q_{\theta}}{\partial \theta}-N_{\theta}+R\,p_{n}=0 \tag{9}$$

$$\frac{1}{R}\frac{\partial M_{x}}{\partial \bar{x}}+\frac{1}{R}\frac{\partial M_{\theta x}}{\partial \theta}+Q_{x}=0 \tag{10}$$

$$\frac{1}{R}\frac{\partial M_{x\theta}}{\partial \bar{x}}+\frac{1}{R}\frac{\partial M_{\theta}}{\partial \theta}+Q_{\theta}=0 \tag{11}$$

being $\bar{x}=\frac{x}{R}$, the dimensionless axial coordinate.

The stress state reaches the highest values around the areas of curvature change. One of the areas where the stresses will need particular attention is around the hemisphere to cylindrical nozzle intersection. Another area where the stresses will be more intense is the intersection between the spherical shell and the cylindrical shell.

The set of equations for spherical and cylindrical shells can be developed in a Fourier series expansion along the intersection curves. The boundary conditions imposed to obtain the stress, strain and displacement fields (Xue, M.D., Li, D.F., Hwang, K.C., 2004).

Another approach is to develop a finite element formulation for the elasto-plastic behavior of thick shells with the inclusion of large rotations. The integration of the generalized stress resultants in the variational form of the strain energy density over the domain of the shell, leads to the element bending stiffness matrix, the element stretching stiffness matrix and the element transverse shear deformation matrix (Voyiadjis, George Z., Woelke, Pawel, 2004b)

3. PRINCIPLE OF VIRTUAL WORK

Equilibrium may be viewed under a general form, when virtual work is considered. The equilibrium of a shell element, under a Lagrange view point, can be expressed as:

$$V=\int_{A_0}(\mathbf{N}^{\mathbf{T}}\delta\mathbf{E}+\mathbf{M}^{\mathbf{T}}\delta\boldsymbol{\kappa}+\mathbf{Q}^{\mathbf{T}}\delta\boldsymbol{\gamma})dA_0-\mathbf{q}^{\mathbf{T}}\delta\mathbf{u} \tag{12}$$

where the in-plane stress resultants $<N_{\alpha},N_{\beta},N_{\alpha\beta}>$ are represented in terms of the thickness t by:

$$\left\lfloor N_{\alpha}\quad N_{\beta}\quad N_{\alpha\beta}\right\rfloor=\int_{t}\left\lfloor S_{\alpha}\quad S_{\beta}\quad S_{\alpha\beta}\right\rfloor dz \tag{13}$$

The moment resultants are obtained by

$$\lfloor M_\alpha \quad M_\beta \quad M_{\alpha\beta} \rfloor = \int_t \lfloor S_\alpha \quad S_\beta \quad S_{\alpha\beta} \rfloor z dz \tag{14}$$

whereas the shear resultants, dependent of the off diagonal terms so that

$$\lfloor Q_\alpha \quad Q_\beta \rfloor = \int_t \lfloor S_{\alpha z} \quad S_{\beta z} \rfloor dz \tag{15}$$

All of them dependent of the second Piola-Kirchhoff stress $\mathbf{S}$. Here $<\alpha,\beta>$ represent in-plane directions of the shell and z the thickness direction coordinate. Several simple shell forms may be described with this form.

Associate with these stress resultants, Green-Lagrange stress components in terms of in-plane displacement components $<U_\alpha, U_\beta>$ and out-of-plane w displacement result:

$$\lfloor E_\alpha \quad E_\beta \quad E_{\alpha\beta} \rfloor = \lfloor U_{,\alpha} + \tfrac{1}{2} w_{,\alpha}{}^2 \quad V_{,\beta} + \tfrac{1}{2} w_{,\beta}{}^2 \quad U_{,\alpha} + V_{,\beta} + w_{,\alpha} w_{,\beta} \rfloor \tag{16}$$

with independent curvature relations:

$$\lfloor \kappa_\alpha \quad \kappa_\beta \quad \kappa_{\alpha\beta} \rfloor = \lfloor \theta_{,\alpha} \quad \phi_{,\beta} \quad \theta_{,\beta} + \phi_{,\alpha} \rfloor \tag{17}$$

being $<\theta,\phi>$ the rotations with respect to the section normals in the $<\alpha,\beta>$ directions. Partial derivatives are indicated in the $\frac{\partial}{\partial x}[\,] = [\,]_{,x}$ form. From these rotations, under a Reissner-Mindlin approach, vertical shear may be expressed in the form:

$$\lfloor \gamma_{\alpha z} \quad \gamma_{\beta z} \rfloor = \lfloor \theta + w_{,\alpha} \quad \phi + w_{,\beta} \rfloor \tag{18}$$

3.1 FEA INTERPOLATION

Five degrees of freedom characterize behavior of the simple shell elements. For points of the shell middle surface, the set $<U,V,w,\theta,\phi>$ provides identification of displacements from in-plane displacements $<U,V>$ plus lateral displacement w and rotations $<\theta,\phi>$. Discretization of the geometry into an assemblage of flat elements where positions in the present configuration are mapped from positions in the initial configuration provide the basis of the Total Lagrange solution. Interpolation of these middle surface variables from nodal values leads to:

$$\begin{aligned} U &= \mathbf{h}_U{}^{\mathbf{T}} \hat{\mathbf{U}} \\ V &= \mathbf{h}_V{}^{\mathbf{T}} \hat{\mathbf{V}} \\ w &= \mathbf{h}^{\mathbf{T}} \hat{\mathbf{W}} \\ \theta &= \mathbf{h}^{\mathbf{T}} \hat{\mathbf{\Theta}} \\ \phi &= \mathbf{h}^{T} \hat{\mathbf{\Phi}} \end{aligned} \tag{19}$$

where the $\lfloor h \rfloor$ vectors (in row form), comprise the interpolation functions. In-plane variables $<U,V>$ in general have a lower order interpolation, and therefore related to particular h-functions. In the above $<\hat{\mathbf{U}},\hat{\mathbf{V}},\hat{\mathbf{W}},\hat{\mathbf{\Theta}},\hat{\mathbf{\Phi}}>$ represent nodal values. Size of the arrays depends on the type of element considered.

Applying the strain-displacement operators, in-plane relations as well as curvature and shear displacements relations may be constructed to produce the variations:

$$\begin{aligned} \delta\mathbf{E} &= \mathbf{B}_E \delta\hat{\mathbf{D}} \\ \delta\boldsymbol{\kappa} &= \mathbf{B}_\kappa \delta\hat{\mathbf{D}} \\ \delta\boldsymbol{\gamma} &= \mathbf{B}_\gamma \delta\hat{\mathbf{D}} \end{aligned} \tag{20}$$

where $<\mathbf{B}_e, \mathbf{B}_\kappa, \mathbf{B}_\gamma>$ are the interpolation matrices. The displacement vector is $\mathbf{D}^{\mathbf{T}} = \lfloor \hat{\mathbf{U}} \quad \hat{\mathbf{V}} \quad \hat{\mathbf{W}} \quad \hat{\mathbf{\Theta}} \quad \hat{\mathbf{\Phi}} \rfloor$. Furthermore the constitutive relation at the depth z, where the strains are $\mathbf{e} = \mathbf{E} + \boldsymbol{\kappa} z$ is of the form;

$$\mathbf{S} = C_e : \mathbf{e} \tag{21}$$

where $\mathbf{C}_e$ is the elastic constitutive equation. From the above, generalized strain expressions, after integration, result:

$$\begin{aligned} \mathbf{N} &= \mathbf{C_m}\mathbf{E} + \mathbf{C}_{mb}\boldsymbol{\kappa} \\ \mathbf{M} &= \mathbf{C}_{mb}{}^{\mathbf{T}}\mathbf{E} + \mathbf{C}_b\boldsymbol{\kappa} \end{aligned} \tag{22}$$

and from PVW, Eq. (12), the tangent stiffness matrix follows in the normal way after appropriate differentiations:

$$\mathbf{K} = \int_{A_0} \lfloor \mathbf{B}_E{}^T \quad \mathbf{B}_\kappa{}^T \quad \mathbf{B}_\gamma{}^T \rfloor \begin{bmatrix} \mathbf{C}_m & \mathbf{C}_{mb} & \mathbf{0} \\ \mathbf{C}_{mb}{}^{\mathbf{T}} & \mathbf{C}_b & \mathbf{O} \\ \mathbf{0} & \mathbf{0} & \mathbf{C_s} \end{bmatrix} \begin{bmatrix} \mathbf{B}_E \\ \mathbf{B}_\kappa \\ \mathbf{B}_\gamma \end{bmatrix} dA + \int_{A_0} \mathbf{B}_s{}^T \begin{bmatrix} N_\alpha & N_{\alpha\beta} \\ N_{\alpha\beta} & N_\beta \end{bmatrix} \mathbf{B_s}\, dA \tag{23}$$

Displacements may be computed directly from the relation, $\mathbf{K}\hat{\mathbf{D}} = \mathbf{F}$, being $\mathbf{F}$ the resultant force from the external loading.

3.2. Finite element modeling

The gas cylinder container was designed for the AISI 4130 steel. The material has tensile strength at yield $S_y = 460\,\text{MPa}$ and ultimate tensile strength $S_u = 560\,\text{MPa}$, Poisson's module $\nu = 0.29$ and machinability of 70%. The container is assumed at a static equilibrium under the internal constant pressure of 20 MPa. For modeling purposes the nozzle end was assumed closed.

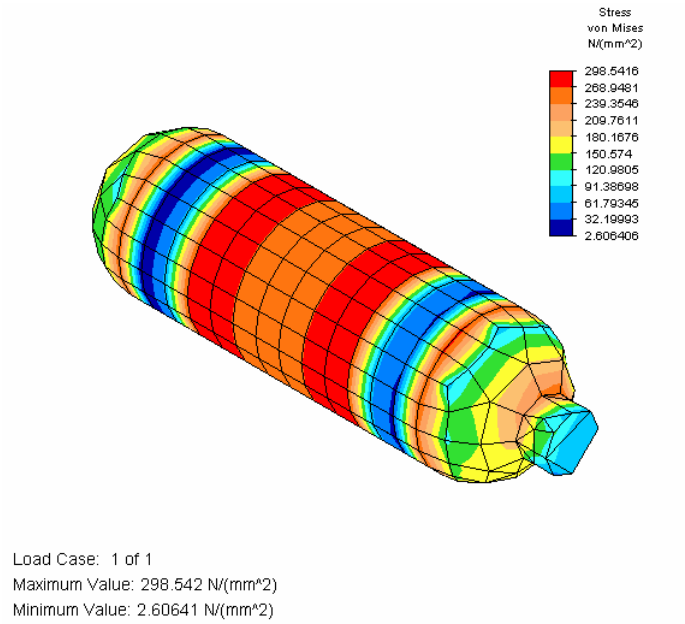

Figure 2 FE shell model and von Mises stresses distribution on the gas container

The hoop stresses on the cylindrical body are in the linear range. For a cylindrical shell of thickness is 10 mm, the hoop stresses, membrane effect, amount to 244 MPa. The hoop stresses are the preliminary design factor on the determination of the minimum shell thickness (Diamantoudis, A. Th., Kermanidis, Th., 2005). A step loading pressurization, with small increments is assumed in order to achieve the final operational pressure. The analysis was performed using Algor Finite Element program and CosmosWorks finite element package.

The first analysis was performed using shell elements. The meshing was medium and the results are presented in Fig. 2. Figure 3 shows the displaced form of the container with an amplification factor of 2.5%. It can be noticed the region where the strips hold the container.

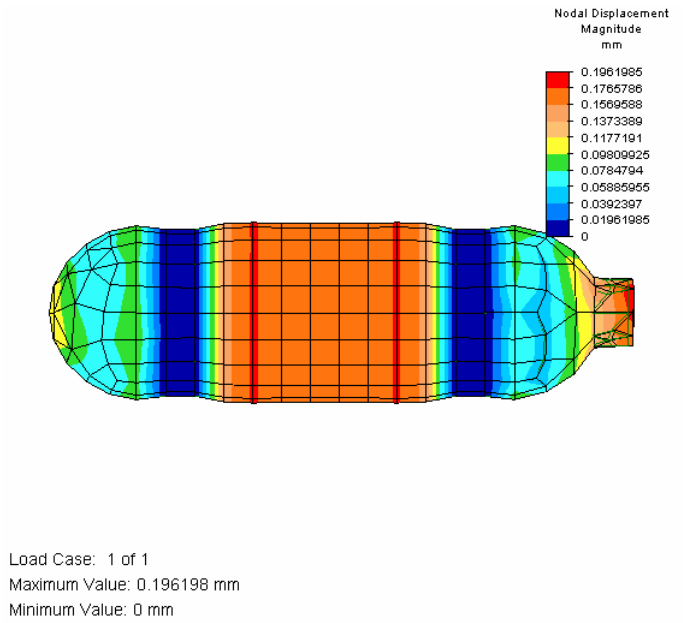

Figure 3 FE shell model and displacements on the gas container.

The region where the cylindrical nozzle intersects the hemisphere requires attention because of stress concentrations. After refining the shell meshing around the nozzle area, we observe the stresses variations on the external surface (Fig. 4) as well as on the internal surface (Fig. 5).

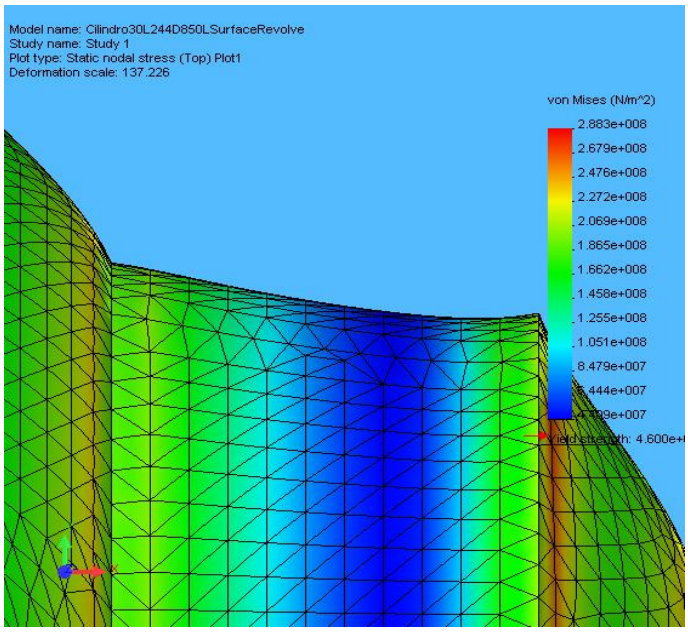

Figure 4 Total external nodal stresses (von Mises) contour plot.
Discrete contour stresses on nozzle area represented on top of deformed shape.

The combined stresses (membrane and bending effects) are considerably different on the bottom (internal) and top (external) surfaces. Figure 4 shows the discrete contour stresses in the proximity of the nozzle and hemisphere intersection. The average stresses are of the order of 230 MPa.

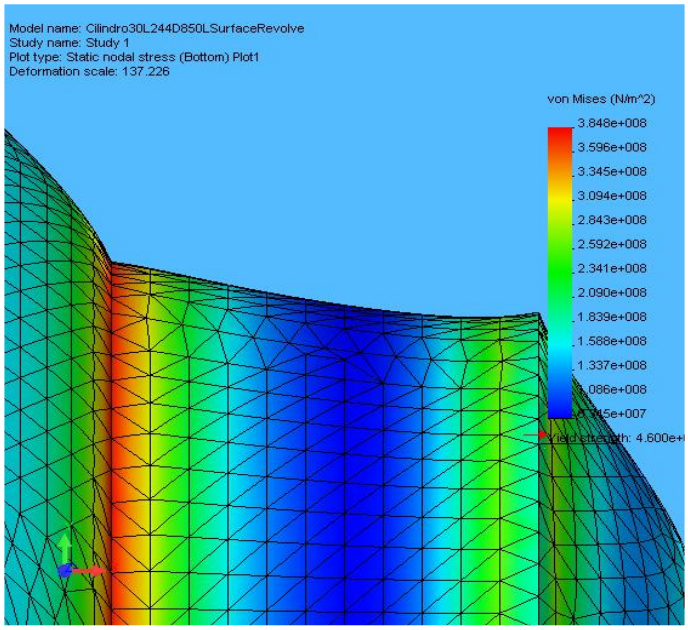

Figure 5. Total internal nodal stresses (von Mises) contour plot.
Discrete contour stresses on nozzle area represented on top of deformed shape.

Figure 5 shows the discrete contour stresses for the same region of the nozzle and hemisphere intersection. However, the stresses are computed on the internal face of the shell. It can be observed that the average stress level is of the order of 350 MPa. In other words, the through thickness stress distribution in non linear.

For the comparison analysis, we used a 3D-solid model with hexahedral solid elements in FE modeling technique.

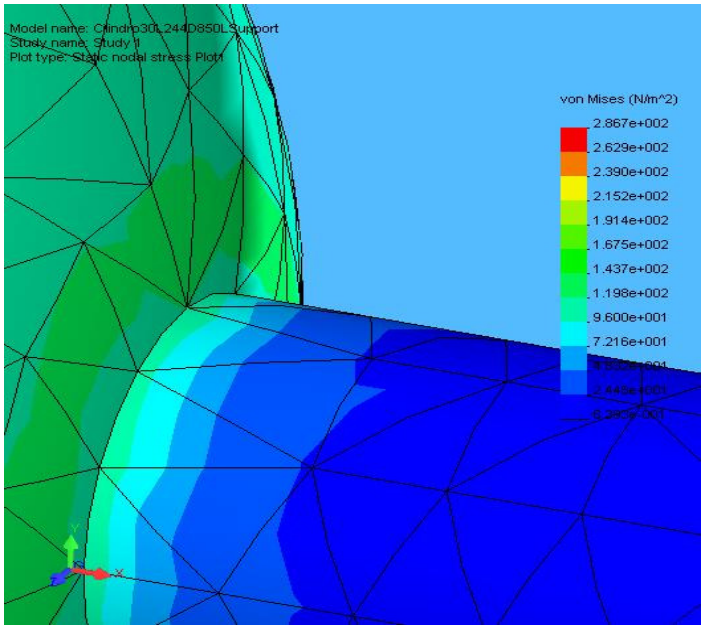

Figure 6. Solid model nodal stresses (von Mises) contour plot.
Discrete contour stresses on nozzle area

The stress level for the cylindrical nozzle and hemispherical area using a solid model is presented in Figure 6. It can be observed that the average stress level is a little lower than the corresponding result using a shell model. Similar conclusions were observed by Diamantoudis, A. Th., Kermanidis, Th., 2005.

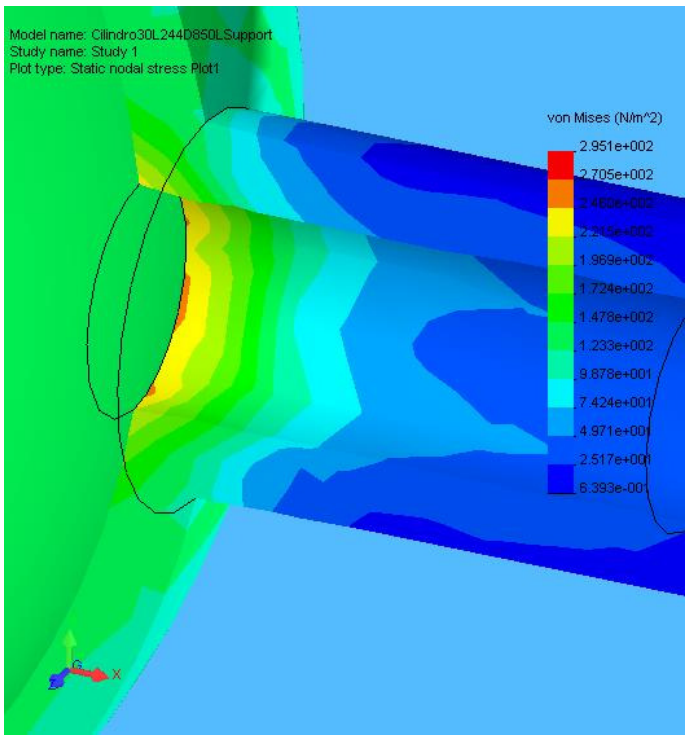

Figure 7 von Mises´s section stresses distribution.
Discrete thickness contour stresses on nozzle area

Figure 7 shows von Mises stresses on a section through the thickness of the solid nozzle. The stress distribution seems to indicate that the plastic region starts developing from the inside to the outside of the nozzle, along the intersection area.

3. CONCLUSIONS

The present investigation confirms the expected stress concentrations on regions of curvature change. The von Mises internal stresses along the intersection curve of the cylindrical nozzle and the hemisphere are close to the yield strength of AISI 4130. The stress level indicates that the plastic deformation is likely to happen around the nozzle sphere intersection. However the stress level obtained by a shell modeling is higher than the results reported by a solid modeling. The solid modeling results conform more closely to the ASME code required safety factor of 1.5. Certainly, experimental data reports would enforce the model results.

4. REFERENCES

Cilibras, 2007, "Catálogo de Cilindros para Gás Natural Veicular – GNV. Especificações de Cilindros para Uso Automobilístico"

Diamantoudis, A. Th., Kermanidis, Th., 2005, " Design by analysis versus design by formula of high strength steel pressure vessels: a comparative study", International Journal of Pressure Vessels and Piping, Vol. 82,pp. 43-50

Dynetek Industries, 2001, http://www.dynetek.com/

Gifel, 2007, "Catálogo de Cilindros para Armazenamento de Gás GNV", http://www.gifel.com.br/

Mannesmann Cylinder Systems, 2007, "CNG Cylinders", MCS International GmbH, http://www.mcs-international-gmbh.de/scripts_en/company/products01.html

Matweb Material Property Data, 2007, http://www.matweb.com/

Sang, Z. F., Xue, L. P., Lin, Y. J., Widera, G.E.O., 2002, "Limit and burst pressures for a cylindrical shell intersection with intermediate diameter ratio", International Journal of Pressure Vessels and Piping, Vol. 79, pp. 341-349

Voyiadjis, George Z., Woelke, Pawel, 2004, "A refined theory for thick spherical shells", International Journal of Solids and Structures, Vol. 41, pp. 3747-3769

Voyiadjis, George Z., Woelke, Pawel, 2006, "General non-linear finite element analysis of thick plates and shells", International Journal of Solids and Structures, Vol. 43, pp. 2209-2242

Xue, M.D., Li, D.F., Hwang, K.C., 2004, "Analytical solution of two intersecting cylindrical shells subjected to transverse moment on nozzle", International Journal of Solids and Structures, Vol. 41, pp. 6949-

Webster, Craig, 2001, "Taking new approaches in standards development for products for new markets", ISO BULLETIN, February, 2001

5. RESPONSIBILITY NOTICE

The authors are the only responsible for the printed material included in this paper.